Int. J. Electrochem. Sci., 8 **(2013)** 2069 - 2079

International Journal of
ELECTROCHEMICAL
SCIENCE
www.electrochemsci.org

Electrochemical Behavior of Corrosion Resistance of X65/Inconel 625 Welded Joints

L.Y. Xu[1, 2], *M. Li*[1, 2], *H.Y. Jing*[1, 2], *Y.D. Han*[1, 2*]

[1] School of Materials Science and Engineering, Tianjin University, Tianjin 300072, PR China
[2] Tianjin Key Laboratory of Advanced Joining Technology, Tianjin 300072, PR China
[*]E-mail: hanyongdian@tju.edu.cn

Received: 11 December 2012 / *Accepted:* 5 January 2013 / *Published:* 1 February 2013

The corrosion resistant alloy of Inconel 625 is cladded on the inner surface of the carbon pipeline steels of X65. Two sections of the corrosion resistant alloy (X65/Inconel 625) were welded by tungsten inert gas welding (TIG) with adding material of ERCrNiMo-3. The electrochemical behavior of the weld metal, heat affected zone (HAZ) and base metal of clad pipe alloys (X65/Inconel 625) was investigated at ambient temperature in 3.5% NaCl solution using potentiodynamic polarization. To reveal the corrosion resistance of different regions in the corrosion resistant alloys welded joints, some significant characterization parameters such as E_{corr}, E_b, I_{corr} and ΔE in polarisation curves were analyzed and compared. The surface morphology of corrosion products was also analyzed by scanning electron microscopy (SEM) and energy-dispersive spectrometer (EDS). The results show that the corrosion resistance of the corrosion resistant alloys in 3.5% NaCl solution at ambient temperature follows the sequence: Root weld＞Upper weld＞Base metal＞Lower HAZ＞Upper HAZ.

Keywords: corrosion resistant alloy; Polarization; Passivity

1. INTRODUCTION

Carbon steel pipelines are widely used in transporting of oil and gas over moderate distances, which are considered as the most cost-efficient solution [1]. It is acknowledged [2-3] that corrosion would cause the failure of pipelines and structural components, resulting in significant economic loss and catastrophic accidents as well as water resource and environmental pollution. Clad pipe provides an economical solution for maintaining a high level of corrosion performance [4]. The rapid development of clad pipe has increased the demand for various types of cladding layer including Inconel 625. This material has outstanding properties to prevent corrosion [5].

X65 pipeline steel is applied widely to large-scale submarine oil and gas pipeline projects [6]. Inconel 625 is a nickel-chromium-molybdenum alloy with an addition of niobium and titanium which acts as stabilizing elements to tie up carbon against sensitization to intergranular corrosion. High corrosion resistance is primarily due to the passivating oxide layered structure that forms on the surface of Inconel 625, which protects the material from further corrosion [7-8].

In order to enhance corrosion resistance of carbon pipeline steels under the seawater environment, corrosion resistant alloys are often cladded on the inner surface of the pipeline steels using the mechanical/metallurgical method. Huet *et al.* [9-10] found that, with a change in oil/brine composition close to the electrode surface, there is a significant fluctuation of the electrolyte resistance and the corrosion of X65 pipeline steel. Studies by Zhang *et al.*[11] on X65 pipeline steel in the simulated oil/water solution under electrochemical conditions confirmed that mass-transfer of oxygen plays a significant role in cathodic process of steel in both oil-free and oil containing solutions. Neville *et al.* [12] showed that the passive film forming on Inconel 625 is a mixed Fe-Cr oxide; and protects the material from further corrosion. The ability of wrought Inconel 625 to exhibit passivation at remarkably low current density values during polarization tests is well established [13].

In the case of welding process, a large amount of heat input can be dissipated via heat conduction throughout the base material close to the welded zone. Typically, this thermal dissipation induces localized isothermal sections where the thermal gradient can have important and detrimental effects on the microstructure and therefore on the mechanical properties and corrosion resistant of the material constituting the heat affect zone (HAZ) and welding seam [14]. However， most studies mentioned above focused on the corrosion behavior of base metal [15], and only few ones considered the welding effect on the corrosion behavior of weld region and heat affected zone (HAZ) of corrosion resistant alloys. So far, to our knowledge, few studies reported the corrosion resistance of different zones in the clad pipe welded joints.

Accordingly in the present study, a new welding procedure was developed according to the welding difficulties of X65/Inconel 625 clad pipe. Then the corrosion behavior of different zones of clad pipe welded joints in the seawater environment by using electrochemical methods was studied. The morphology of corrosion products of pipeline steels Inconel 625 and X65 was carried out using scanning electron microscopy (SEM) and energy-dispersive spectrometer (EDS). The corrosion products were also qualitatively analyzed by X-ray diffraction (XRD).

2. EXPERIMENTAL

The nominal chemical composition of API 5LD (X65 +Inconel 625) clad Pipe for welding are given in Table 1. X65 steel pipe of 219.1mm O.D. and 12.7+3mm thickness with suitable V-groove preparation was used for tungsten inert gas welding (TIG) with add material of ERCrNiMo-3. Welding procedure was performed in 14 passes by the manual gas tungsten arc welding process. The welding parameters and the heat input in each welding pass are given in Table 2 (a) and (b). The butt joint geometry and welding passes sequences are illustrated in Fig. 1 (a) and (b), respectively.

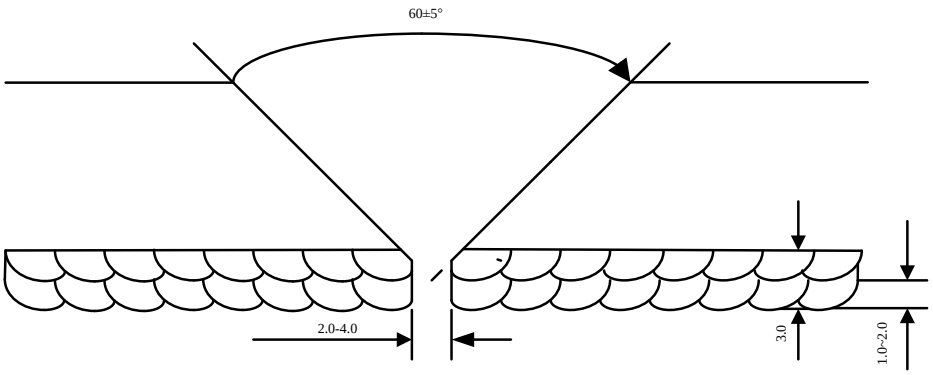

(a) Inconel 625 and X65 pipelines joint geometry of the single-v-groove weld

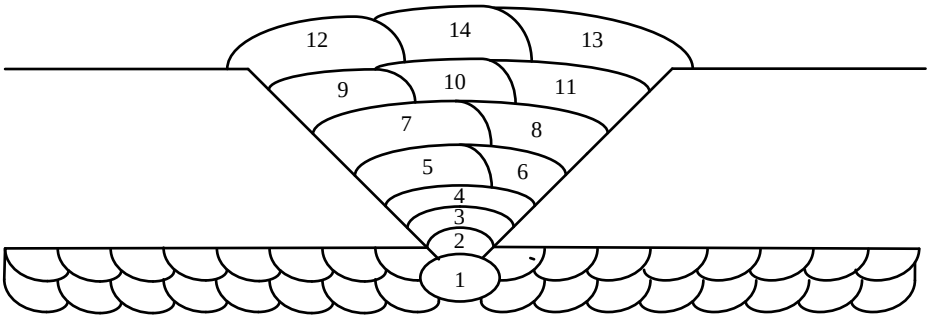

(b) The passes sequences of TIG

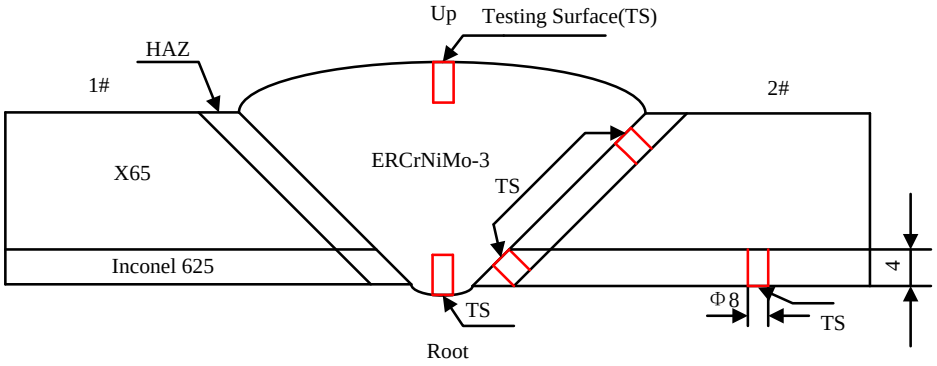

(c) Schematic diagram of sampling different zones in the welded joints for electrochemical corrosion test

Figure 1. The schematic cross-section of specimens cut down from the pipeline

Table 1. The chemical compositions of corrosion resistant alloys tested

Specimens	Elements (wt.%)											
	C	S	Si	Mn	P	Ni	Cr	Mo	W	Ti	Nb	Fe
X65	0.07	0.005	0.3	1.5	0.01	0.004	0.2	≤0.3	≤0.1	0.02	0.06	Bal.
Inconel 625	0.026	0.0012	0.14	0.087	0.005	59.87	21.94	9.02	0.14	0.26	3.44	Bal.

The different zones were cut from the welded joint using wire cutting. The sampling of different zones such as base metal, upper weld, root weld, upper HAZ and lower HAZ in the welded

joint for the electrochemical corrosion experiments was schematically shown in Fig. 1 (c).Then the corrosion resistance in different zones of welded joints was evaluated. The specimens wereφ8×4mm rods embedded in silica gel with an exposed working area of 0.502 cm^2.

Table2. (a) The TIG welding parameters used in this study

Welding parameters	Specific values
Heat Number	H456110621
Welding Amps(A)	90-180
Welding Arc Volts(V)	12-14.5
Tungsten Electrode Size	φ2.4mm
Travel Speed	34-129mm/min
String or Weave	String and weave
Time lapse between SB-HP	Max.10 min
Single or Multipass	Multipass
Single or Multiple Arcs	Single
Root Treatment	Grinding by Stainless steal wheels

Table 2. (b) The TIG welding parameters was performed in 14 passes.

Weld Layers	Welding Process	Welding current		Arc Voltage (V)	Gas Type	Gas flow Rate (L/min)	Finish Time (Min)	Travel Speed (mm/min)	Heat input (KJ/mm)	Preheat & Interpass Tem (℃)
		Type & Polarity	Amps (A)							
1	TIG	DC(-)	90	12	Ar	15-18	20.50	34	1.93	45
2	TIG	DC(-)	135	13	Ar	15-18	5.35	129	0.82	56
3	TIG	DC(-)	135	13	Ar	15-18	7.65	90	1.17	78
4	TIG	DC(-)	145	13	Ar	15-18	8.30	83	1.37	100
5	TIG	DC(-)	145	13	Ar	15-18	8.10	85	1.33	110
6	TIG	DC(-)	145	13	Ar	15-18	7.30	94	1.20	120
7	TIG	DC(-)	180	14.5	Ar	15-18	6.10	113	1.39	65
8	TIG	DC(-)	180	14.5	Ar	15-18	7.10	97	1.62	76
9	TIG	DC(-)	180	14.5	Ar	15-18	5.90	117	1.34	92
10	TIG	DC(-)	180	14.5	Ar	15-18	7.80	88	1.78	115
11	TIG	DC(-)	180	14.5	Ar	15-18	7.70	89	1.75	60
12	TIG	DC(-)	145	13	Ar	15-18	7.60	90	1.25	90
13	TIG	DC(-)	145	13	Ar	15-18	7.20	96	1.18	110
14	TIG	DC(-)	145	13	Ar	15-18	6.90	100	1.13	115

Before test, chemical rinsing was used to remove the oil and rust on the surface of the specimens. The specimens were then cleaned by acetone and deionized water and dry in air. The specimens were ground by silicon carbide abrasive papers of grit 240, 600, 800, 1000 and 1500, respectively. After that, the specimens were dried and placed in the test cell. The electrochemical measurement experiments were conducted with a typical three-electrode cell. Potentiodynamic polarization measurements were carried out in the CS150 Electrochemical & Corrosion Workstation (China) at ambient temperature and the solution was 3.5% NaCl. A saturated calomel electrode (SCE) and platinum (Pt) counter electrode were used as the counter and reference electrodes, respectively. For dynamic polarization testing, the scanning range was from −2.0 V_{SCE} to 2.0 V_{SCE}, and the scanning

rate was 0.2 mV/s. Working electrodes were initially reduced potentiostatically at −1.0 V_{SCE} for 20 min in order to remove air-formed oxides before anodic polarization measurement.

The surface and morphology were analyzed using Scanning Electron Microscopy (SEM) and Energy-dispersive spectrometer (EDS). The corrosion products were also qualitatively analyzed by X-ray diffraction (XRD).

3. RESULTS AND DISCUSSION

3.1 Potentiodynamic polarization

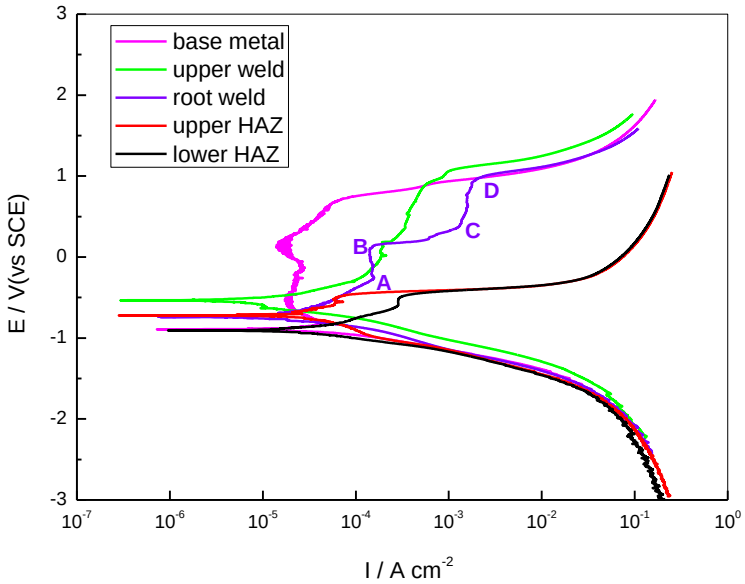

Figure 2. Potentiodynamic polarisation curves obtained as a function of various corrosion resistant alloys exposed in 3.5% NaCl solution at ambient temperature.

Fig. 2 shows the potentiodynamic polarization curves of the Inconel 625 base metal, the weld metal and HAZ of each specimen in 3.5% NaCl solution at ambient temperature. From the polarization curves, the corrosion potential (E_{corr}), the breakdown potential (E_b), and the dynamic corrosion current density (I_{corr}) were determined (See Table 3). It can be observed that all specimens show the passivation regions. The base metal and welding seam indicate stable passivation regions while HAZ showed poor passivation behavior. By comparing the corresponding values of these parameters for the base metal, welding seam and HAZ samples, it can be observed that welding with add material of ERCrNiMo-3 increased the corrosion resistance as expected. The difference between the breakdown potential and the corrosion potential for the corrosion system can be defined as the width of the passive region, i.e., $\Delta E = E_b - E_{corr}$. The width of the passive region on the anodic polarization curves (ΔE) indicates the pitting resistibility or the stability of the passive film, that is, the higher the ΔE value, the more stable of the passive film [8]. It is clear that the ΔE values of the welded joints follow the

sequence (in deceasing order): Root weld＞Upper weld＞Base metal＞Lower HAZ＞Upper HAZ. Based on the above results, it can be concluded that the pitting corrosion resistance of welded joints follows the sequence(in deceasing order): Root weld＞Upper weld＞Base metal＞Lower HAZ＞Upper HAZ. In addition, only the polarization curve of root weld possessed two passivity platforms at the anodic region among the five curves.

Table 3. Corrosion properties for corrosion resistant alloys exposed in 3.5% NaCl solution at ambient temperature

Specimens	E_{corr} (mV_{SCE})	E_b (mV_{SCE})	$\triangle E$ (mV)	I_{corr} ($\mu A/cm^2$)
Base metal	-893.2	671.1	1564.3	28.16
Upper weld	-535.1	1062.9	1598.0	19.68
Root weld	-736.2	992.1	1728.3	12.31
Upper HAZ	-721.1	-433.5	287.6	83.82
Lower HAZ	-905.6	-468.9	436.7	76.77

It suggests that the larger test driving force was required to initiate the corrosion of the root weld. Passvation first took place at point A and then broke down at point B. The second passive stage appeared between point C and D. The corrosion current densities were obtained by using the *Rp* extrapolation method. The magnitude of corrosion current densities (I_{corr}) is considered as an indicator of corrosion resistance, that is, the smaller the I_{corr} value, the more stable of the specimen. The corrosion current densities (I_{corr}) of Base metal, Upper weld, Root weld, Upper HAZ and Lower HAZ were 28.16 $\mu A/cm^2$, 19.68 $\mu A/cm^2$, 12.31 $\mu A/cm^2$, 83.82 $\mu A/cm^2$ and 76.77 $\mu A/cm^2$, respectively. Root weld presented the widest passive potential range and smallest corrosion current densities, which suggests that the root weld has the best pitting corrosion resistance [8, 16].

The results can be attributed to the difference of chemical compositions of corrosion resistant alloys (Table 1). Due to the excellent metallurgical compatibility of the various alloying elements such as Cr, Ni, and Mo, these alloying elements give good corrosion resistance for handling the extreme corrosive environments in the process of oil and gas transmission [16-17]. Concerning Mo addition, this element enhances the pitting corrosion resistance of Inconel 625 studied in 3.5% NaCl, reducing progressively the corrosion rate, increasing values of E_b .and $E_{corr.}$ [18] The presence of Ni and Cr elements to form oxides of these two elements, these oxides have high corrosion resistance. Conversely, Mn exerted an opposite effect, mainly due to the presence of MnS inclusions which acted as pitting initiators [19]. When base metal one and two were welded together with add material of ERCrNiMo-3, accompanied by the diffusion of chemical elements. Thus, high Cr, Ni and Mo content and low-Mn content welding seam have better corrosion resistance compared with base metal and HAZ [20].

3.2 Surface morphology

Figs. 3 (a, b, c, d and e) presents the SEM micrographs of the Base metal, the Upper weld, Root weld, Upper HAZ and Lower HAZ region of each specimen after electrochemical corrosion in 3.5% NaCl solution at ambient temperatures, respectively. After electrochemical corrosion, as shown in Fig. 3 (a), only a few sub-micron pits were observed on the as-received base metal samples. The SEM morphology of base metal indicates that the microstructure of the electrochemical corrosion surface of Inconel 625 alloy is different from that of the welding seam and HAZ.

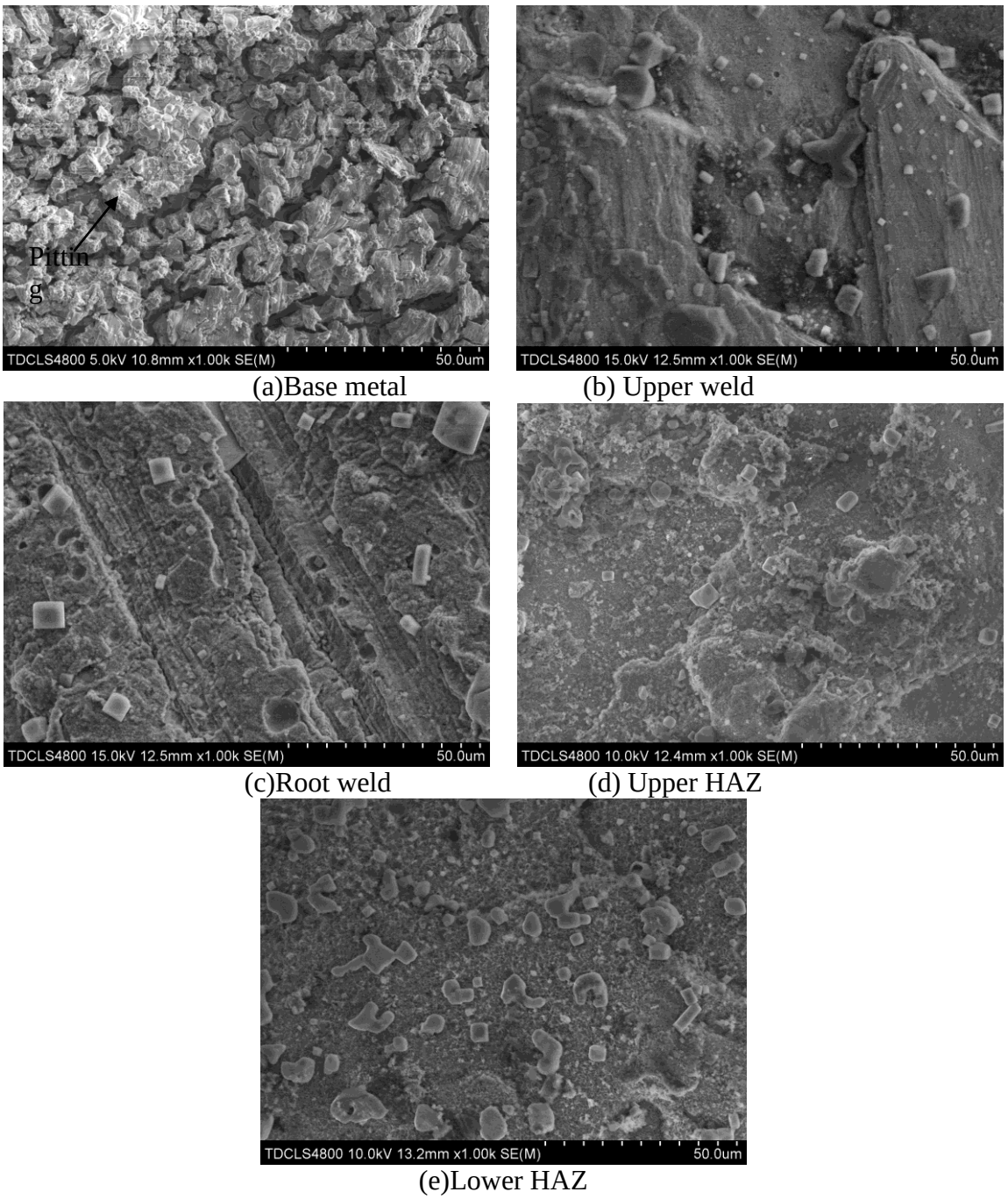

(a)Base metal (b) Upper weld

(c)Root weld (d) Upper HAZ

(e)Lower HAZ

Figure 3. Surface morphology of the specimens

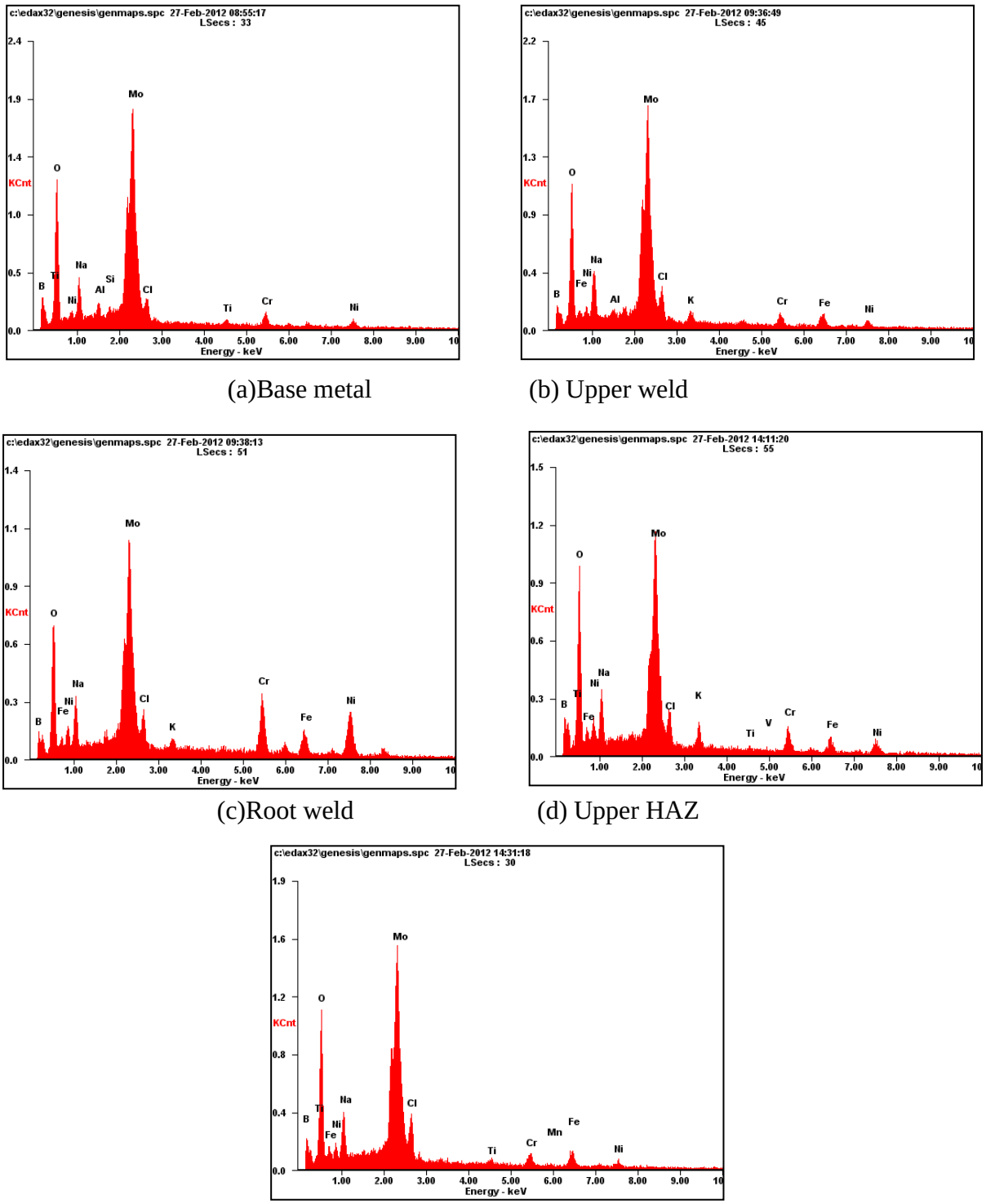

(a)Base metal (b) Upper weld

(c)Root weld (d) Upper HAZ

(e)Lower HAZ

Figure 4. EDS analysis of corrosion product of the specimens after polarization tests

It can be observed that besides base metal, the features of eroded surface of other four target specimens are characterized by the formation of electrochemical corrosion products，which had a square-like shape. The welding seam exhibited superior corrosion resistance when compared to base

metal and HAZ due to its corrosion products were combined more close with matrix than base metal and HAZ.

The amount of corrosion product formed on the surface of welding seam was also more than that on the surface of base metal and HAZ region, which agrees well with the results of potentiodynamic polarization curves in Fig. 2.

Fig. 4 shows the surface element concentrations of corrosion products from EDS. The corrosion products of base metal, the welding seam and HAZ region of each specimen were found to contain main part of O and Mo and small part of Cr and Ni. It is consistent with the results reported in literatures [21-23].

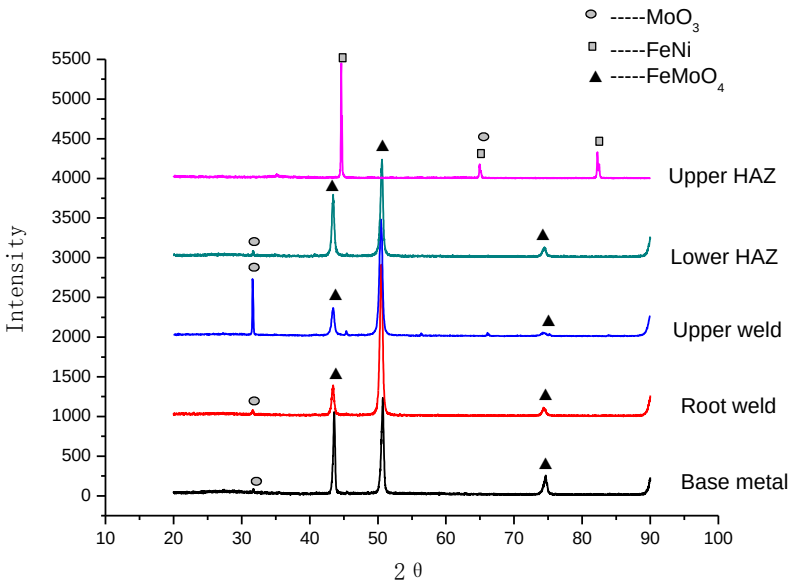

Figure 5. XRD analysis of corrosion product of the specimens after polarization tests

In order to understand the reaction during the corrosion, XRD were used to analysis the corrosion products on the surface after the polarization tests. Fig. 5 shows the XRD analyses of the corrosion products on the surface of base metal, the welding seam and HAZ region of each specimen after the polarization test. Besides upper HAZ, other specimens all had the same corrosion products of MoO_3 and $FeMoO_4$. Observation of Fe, Mo and Ni suggests the presence of FeNi and MoO_3 as previously determined by XRD analysis of upper HAZ. Mo improves the repassivation behavior or the deactivation of growing pits [24]: Ilevbare and Burtstein [25] have showed that the presence of Mo in stainless steels reduced the number and size of both nucleation and metastable pits, decreasing the probability of generating stable pits. Several works defend that Mo promotes the repassivation process by forming insoluble molybdenum chloride complexes [26-27] or MoO_4^{2-} in the active sites. In fact, Sugimoto and Sawada [28] considered that the adsorption of MoO_4^{2-} in pits could inhibit the early stages of pit growth. This MoO_4^{2-} layer is caution selective, and resists the incorporation of anions such as Cl^- allowing for the growth of a Mo oxide outer barrier layer [20]. By contrast, MoO_3 is more

stable than $FeMoO_4$; as a result, its formation is favored within the pit. According to this, the kind of Mo oxides formed may depend on the local zone of the pit where this element is reacting. On the other hand, MoO_3 should be the main compound involved within the repassivation process [18]. Observed from Potentiodynamic polarisation curves (Fig. 2), only root weld have the repassivation process due to the highest content of MoO_3 compared with other specimens (See Fig. 3). The passive layer formed on Inconel 625 is thus believed to mainly consist of Molybdenum oxide. Therefore, the decrease in transpassive potential can be attributed to the effect of MoO_3.

The EDS and XRD results from the present study also suggest that the improved corrosion resistance of alloys might be due to the formation of MoO_3 and $FeMoO_4$ film on the surface. It can therefore be concluded that an increase in molybdenum content of Cr-Ni-Mo alloys increases the corrosion resistance owing to enhancement of the formation of a molybdenum- enriched passive film [29].

4. CONCLUSIONS

The electrochemical corrosion parameters such as E_{corr}, E_b, ΔE and I_{corr} are used to describe the corrosion resistance to 3.5% NaCl solution environment at ambient temperatures. The corrosion potential (E_{corr}) of lower HAZ is the most negative among all the corrosion resistant alloys. The breakdown potential (E_b) of upper weld is the most positive. The corrosion passivation current density (I_{corr}) of root weld is the most negative which has the best resistance to pitting corrosion. The width of passivation regions follows the sequence: Root weld＞Upper weld＞Base metal＞Lower HAZ＞Upper HAZ.

The corrosion product on the surface of base metal, the welding seam and HAZ region studied after potentiodynamic polarization tests in 3.5 wt. % NaCl solution environments at ambient temperatures were MoO_3, which had a square-like shape and was loosely distributed on the surface with different orientations. The enriched Mo layer acts as a barrier to the dissolution/oxidation of Inconel 625 and X65 and thereby limits the corrosion current rate within the passive region.

ACKNOWLEDGEMENTS
The authors acknowledge the research funding by National Natural Science Foundation of China (Grant Nos. 50975196 , 51275341, 51205282 and, Key Project in the Science & Technology Pillar Program of Tianjin (Grant No. 11ZCKFGX03000) and, Program for New Century Excellent Talents in University (NCET) and Specialized Research Fund for the Doctoral Program of Higher Education of MOE (Grant No. 20110032130002)

References

1. Choi Yoon-Seok, Choi Srdjan nesic, and David Young,: *Environ. Sci. Technol*, 44 (2010) 159.
2. Damian A. Lopez, S.N. Simison, and S.R. de Sanchez,: *Electrochim. Acta*, 48 (2003) 845.
3. M.B. Kermani, and A. Morshed,: *Corros. Sci.*, 59 (2003) 659.
4. Yoshimi Watanabe, Yoshifumi Inaguma, and Hisashi Sato,: *Mater. Lett.*, 65 (2011) 467.

5. T. Kannan and N. Murugan,: *J. Mater. Process, Technol.*, 76 (2006) 230.
6. E. Gamboa, V. Linton, and M. Law,: *Int. J. Fatigue*, 30 (2008) 850.
7. Darren A .Walsh, Lisa E.Li, M.S. Bakare, and K.T.Voisey,: *Electrochim. Acta*, 54 (2009) 4647.
8. Z.F. Yin, W.Z. Zhao, W.Y. Lai, and X.H.Zhao,: *Corros. Sci.*, 51 (2009) 1702.
9. H. Bouazaze, F. Huet, and R.P. Nogueira,: *Electrochim. Acta*, 50 (2005) 2081.
10. F. Huet, and R.P. Nogueira, *Corros. Sci.*, 50 (2003) 748.
11. G. A. Zhang, and Y. F. Cheng,: *Corros. Sci.*, 51 (2009) 901.
12. A. Neville, M. Reyes, T. Hodgkiess, and A. Gledhill, *Wear*, 238 (2000) 138.
13. N. Ahmed, M.S. Bakare, D.G. McCartney, and K.T. Voisey,: *Surf. Coat. Technol.*, 204 (2010) 2294.
14. P.R. Ambriz, D. Chicot, N. Benseddiq, G. Mesmacque, and S.D. de la Torre,: *Eur. J. Mech. A Solids*, 30 (2011) 307.
15. Stephen E. Ziemniak, and Michanel Hanson,: *Corros. Sci.*, 48 (2006) 498.
16. Z.F. Yin, W.Z. Zhao, W. Tian, Y.R. Feng, and C.X. Yin,: J. *Solid State Electrochem.*, 13 (2009) 1291.
17. H.X. Hu, Y.G.Zheng, and C.P. Qin,: *Nucl. Eng. Des.* 240 (2010) 2721.
18. A. Pardo, M.C. Merino, A.E. Coy, F. Viejo, R. Arrabal, and E. Matykina,: *Corros. Sci.*, 50 (2008) 1796.
19. R. Bandy, and D.Van Rooyen ,: *Corros. Sci.*, 39 (1983) 227.
20. Amy C. Lloyd, James J. Noel, Stewart McIntyre and David W. Shoesmith, *Electrochim. Acta*, 49 (2004) 3015.
21. R. Norling, and I. Olefjord,: *Wear*, 254 (2003) 173.
22. S.R. Allahkaram, P. Zakersafaee, and S.A.M. Haghgoo,: *Eng. Fail. Analysis*, 18 (2011)1108.
23. Janusz Adamiec,: *Mater. Charact.*, 60 (2009) 1093.
24. L.Wegrelius, F. Falkenberg, and I. Olefjord,: *Electrochem. Soc.*, 146 (1999) 1397.
25. G.O. Ilevbare, and G.T. Burstein, *Corros. Sci.*, 43 (2001) 485.
26. A. Schneider, D. Kuron, S. Hofman, and R. Kirchheim,: *Corros. Sci.*, 31 (1990) 191.
27. I. Olefjord, and L. Wegrelius, : *Corros. Sci.*, 38 (1996) 347.
28. K. Sugimoto, and Y. Sawada,: *Corros. Sci.*, 32 (1976) 347.
29. Koji Hashimoto, Pyeong-Yeol Park, Jin-Han Kim, Hideaki Yoshioka, Hiroyuki Mitsui, Eiji Akiyama, Hiroki Habazaki, Asahi Kawashima, Katsuhiko Asami, Zbigniew Grzesik, and Stanislaw Mrowec,: *Mater. Sci. Eng.*, 198 (1995) 1.